

RSC Advances



This is an *Accepted Manuscript*, which has been through the Royal Society of Chemistry peer review process and has been accepted for publication.

Accepted Manuscripts are published online shortly after acceptance, before technical editing, formatting and proof reading. Using this free service, authors can make their results available to the community, in citable form, before we publish the edited article. This *Accepted Manuscript* will be replaced by the edited, formatted and paginated article as soon as this is available.

You can find more information about *Accepted Manuscripts* in the [Information for Authors](#).

Please note that technical editing may introduce minor changes to the text and/or graphics, which may alter content. The journal's standard [Terms & Conditions](#) and the [Ethical guidelines](#) still apply. In no event shall the Royal Society of Chemistry be held responsible for any errors or omissions in this *Accepted Manuscript* or any consequences arising from the use of any information it contains.

Iron — silver oxide nanoadsorbent synthesized by co-precipitation process for Fluoride removal from aqueous solution and its adsorption mechanism

Ali Azari¹, Roshanak Rezaei Kalantary², Babak Kakavandi³, Mahdi Farzadkia², Ehsan Ahmadi¹, Ghader Ghanizadeh⁴

1. Department of Environmental Health Engineering, School of Public Health, Tehran University of Medical Sciences, Tehran, Iran

2. Department of Environmental Health Engineering, School of Public Health, Iran University of Medical Sciences, Tehran, Iran

3. Department of Environmental Health Engineering, School of Public Health, Ahvaz, Jundishapur University of Medical Sciences, Ahvaz, Iran.

4. Department of Environmental Health Engineering, Health Research Center, Baqiyatallah University of Medical Sciences, Tehran, Iran

* **Correspondence:** Ghader Ghanizadeh, Department of Environmental Health Engineering, Health Research Center, Baqiyatallah University of Medical Sciences, Tehran, Iran

P. O. Box: 6446-14155, Tehran1471613151, I.R. Iran, Phone No.: +98 21, 88779118, Fax: +98 21 88779487

E-mail: qanizadeh@bmsu.ac.ir

Abstract

Fe-Ag magnetic binary oxide nanoparticle (Fe–Ag MBON) are prepared with co-precipitation of ferric and ferrous chloride solution, and used for the adsorption of Fluoride from aqueous solution. The surface morphology of adsorbent was characterized by XRD, SEM, TEM, FTIR, XPS, EDX, BET, DLS and VSM techniques. Batch method was followed to optimize the conditions for the removal of Fluoride. The results showed maximum removal was occurred at pH 3.0 and adsorption equilibrium was achieved within 20 min. Chemical kinetics of the adsorption were well fitted by pseudo-second order models ($R^2 > 0.968$) and the adsorption process followed the Langmuir isotherm model well ($R^2 > 0.976$). The Fluoride adsorption capacity of Fe–Ag MBON were 22.883 mg/g, and decreased with increasing the temperature. Thermodynamic values revealed that the Fluoride adsorption process was spontaneous and exothermic. Regeneration experiments were carried out for six cycles and the results indicate a removal efficiency loss of < 22%.

Keyword: Fluoride Adsorption, Iron and silver, magnetic binary oxide nanoparticle, Hydroxyl group

1. Introduction:

Fluoride (F^-) has been recognized as one of the serious problem in surface/ground water [1]. Different minerals (e.g., fluorite, biotites, topaz) are the natural geological sources of Fluoride which can be released into the groundwater[2]. Moreover various industries such as glass and ceramic production, fertilizer and semiconductor manufacturing are also contributing in fluoride pollution to a large extent. The effluents of these industries may be reached to thousands mg/L which higher than natural waters[3]. Depending on the concentration and water temperature, the effect of fluoride in drinking water can be beneficial or harmful to mankind[4]. Presence small quantities of Fluoride in ingested water are often considered to have a beneficial effect on human health and helps in the normal mineralization of bones and dental formation[5]. On the contrary, excessive intake of fluoride leads to osteoporosis, Alzheimer syndrome, skeletal fluorosis, cancer, infertility, and thyroid disorder[6]. There are some literatures indicating that excess concentrations of fluoride can interfere in DNA synthesis and mineral metabolism[7]. WHO(1984) reported that > 260 million people in the world consume drinking water with a Fluoride content more than acceptable limits (1.5 mg/ L) and in the tropical countries Fluoride concentration can be as high as 35 mg/L naturally[8]. Under these circumstances for the safeguard the environmental and human health, it is necessary to find out suitable material as well as methodology for the sustainable removal to bring down the fluoride levels to acceptable limits. The defluoridation techniques can be mainly classified into three categories, membrane process (verse osmosis, nanofiltration, dialysis and electro-dialysis), chemical process, and adsorption techniques.[9] However, the shortcomings of membrane and chemical process are high operational and maintenance costs, require to pretreatment, regeneration, waste disposal, and secondary pollution[10]. Among these available approaches, adsorption method is widely used and offers satisfactory results due to its cost effective, high efficiency, simplicity of design, reusability and reliable alternatives[11]. Studies of late focus on searching for various sorbents with low cost and high efficient for fluoride removal including activated alumina[12], zeolite[13], hydroxyapatite[14], clay[15], modified chitosan beads[16]. More and more attentions has been paid on the development of new sorbents with high selectivity toward fluoride ion, synthetic materials is strong candidates in this field[17]. Iron oxides are regarded as well-known adsorbent due to their high affinities toward inorganic pollutant, high selectivity in sorption processes, low-cost and environmental friendliness [18, 19]. In recent years, increasing efforts have been devoted to the synthesis the composite adsorbents (containing iron oxides) for removal of inorganic pollutant due to their extensive potential applications. For instances, Fe–Al–Ce[20], Fe–Cu [21], Fe–Al [22], Fe–Zr [23], Fe–Ti [24] have been reported for Fluoride removal. These composites exhibited superior adsorption performance for Fluoride removal than their individual components (Their parent materials)[25]. Previous study showed that Ag oxides derived sorbent had selective potential and good performance in Phosphorus [26], Poly vinyl pyrrolidone (PVP)[27], and color removal from water over a wide pH range[28]. However, applied pure silver oxides as sorbent it is not economical due to its high cost. To save costs, some composite adsorbents comprising silver oxides have therefore been developed. However, up to now, removal of Fluoride by Fe–Ag as an adsorbent has not been reported in the literature, although they are maybe an excellent adsorbent because used from both Fe and Ag oxides simultaneous benefits. Besides, combination the silver oxide with high cost (US ~ \$ 5000–15,000 /Ton) and iron oxide with low price (US ~\$500–1000/Ton) would remarkably lower the adsorbent cost. Therefore, The main objectives of this study summarized in (1) to synthesize Fe–Ag MBON with different Fe/Ag molar ratios and its characterization by XRD, SEM, TEM, FTIR, XPS, EDX, BET, DLS and

VSM techniques; (2) Investigate the efficiency of newly synthesized Fe–Ag MBON for Fluoride removal from the aqueous solution with considering impact of various experimental parameters such as pH, temperature, adsorbent dose, contact time and initial Fluoride concentrations (3) The equilibrium isotherm and kinetic modeling and thermodynamics of Fluoride adsorption process in batch system and finally (4) to investigate the mechanism for Fluoride removal.

2. Experimental

2.1. Materials and Instruments

Ferrous sulfate heptahydrate ($\text{FeSO}_4 \cdot 7\text{H}_2\text{O}$, 99%), Ammonia (NH_3), AgNO_3 (>99.0%) were purchased from Merck Company and were used as received without further purification. In this study for pH adjustment implied hydrochloric acid (HCl, 35-37%) and sodium hydroxide (NaOH, 93%). Sodium fluoride (NaF , 99% sigma-Aldrich) used for preparation Fluoride stock solution in deionized water. All chemicals used in this study were analytical grade. pH meter (HACH-HQ-USA) and incubator shaker (VWR1535) were used to measure of pH solutions and adjust temperature and stirring rate, respectively.

2.2. Synthesis and Characterization of Fe–Ag MBON

A series of Fe–Ag MBON were synthesized under various Fe/Ag molar ratios by co-precipitation method base on the procedure described by Chen et al with little difference. [24] Predetermined amount of $\text{FeSO}_4 \cdot 7\text{H}_2\text{O}$ and AgNO_3 were dissolved in 500 ml deionized water. Under vigorous mechanical stirring, 12.5% ammonia solution was added dropwise to reach the solution pH to 9.5. The Fe/Ag molar ratio was regulated to the predetermined value by changing in the amount of $\text{FeSO}_4 \cdot 7\text{H}_2\text{O}$ or AgNO_3 added. After reaction, the black suspension (Fe–Ag) was stirred at the 80°C for 1 h. Then Fe–Ag MBON were separated from the solution by external magnetic field and washed several times with distilled water. Fe–Ag MBON dried at 45°C for 12 h and stored in a desiccator.

The obtained material appeared in the tiny powder form, which were named as Fe/Ag A: B (A: B = 1:0, 3:1, 1:1, 1:3 and 0:1. A: B means the molar ratio of $\text{FeSO}_4 \cdot 7\text{H}_2\text{O}$ and AgNO_3).

2.3. Adsorbent characterization

The surface morphological properties of Fe–Ag MBON was observed by scanning electron microscope (SEM, PHILIPS, S360, and Mv2300). Structural analysis of an adsorbent and the information of various functional groups in the adsorbent were conveyed by Fourier transform infrared spectroscopy with spectral grade KBr in an agate mortar (FTIR, FTS-165, BIO-RAD, USA). The elemental and structural composition were analyzed by energy dispersive X-ray (EDX, PHILIPS, S360, and Mv2300) before and after adsorption. The binding energies of the elements and specific functional groups before and after adsorption were obtained by using X-ray Photoelectron Spectroscopy with a monochromatic Al K-alpha X-ray source (1486.6 eV) (XPS, AXIS 165 (Kratos)). Particles size, shape and size distribution analysis of synthesized adsorbent analyzed by transmission electron microscopy (TEM, PHILIPS, EM 208 S 100KV). X-ray Diffraction (XRD, Quanta chrome, NOVA2000) and Vibrating sample magnetometer (VSM, Lakeshore 7307) used for the study of composition crystalline structures of Fe–Ag MBON and magnetic separation ability of sorbent, respectively. Dynamic light scattering particle size analysis was performed to determine the particle size distributions of Fe and Ag oxides (DLS, SZ-100

nanopartica series). Nitrogen adsorption and desorption analysis was used to study the specific surface area and pore structure of Fe–Ag MBON samples (NOVA 2200 - Quantachrome Corp. USA). The point of zero charge (pzc) for Fe–Ag MBON was determined by plotting as final pH–initial pH (pH_f–pH_i) versus pH, yielded the pzc as the pH where pH_f–pH_i = 0 according to the method described by Zhang et al. [29]

2.4. Batch adsorption experiments

Fluoride adsorption experiments by prepared Fe–Ag MBON carried out in batch condition and experimental scale in 100 ml flask while shaking on a shaker-incubator at 180 RPM. The stock solution of Fluoride was prepared by dissolving 2.2 g NaF in 1000 ml deionized water and with dilution of stock solution the other concentrations of Fluoride were prepared. The pH of solution (3–13), Fe–Ag MBON dosage (0.1–1 g/L), Fluoride concentration (5–30 mg/L) and contact time (0–60 min) selected as variables in this research. To deliver the pH to the desired range was applied from 0.1N HCl and NaOH solutions. After the adsorption process and separating the adsorbent, the supernatant solution was collected for the residual Fluoride concentration and analysis in the UV-visible scope at the maximum adsorption ($\lambda = 580$ nm) by using spectrophotometer UV-Vis 7400CE CECIL in presence of SPANDS reagents (Procedure of 4500 F⁻ standard method). All experiments were duplicating and average value is presented to ensure the reliability of the results. The amount of Fluoride adsorbed onto the prepared MBON and the removal percentage (%) was calculated through the equation (1) or (2):

$$q_e = \left(\frac{C_0 - C_e}{m} \right) \times v \quad (1)$$

$$r(\%) = \frac{C_{des}}{C_{ads}} \times 100 \quad (2)$$

Here: C_0 and C_e are initial and equilibrium concentrations of F⁻ (mg / L) respectively, V the volume of solution (L), and M is the mass of adsorbent (g) requirements.

For the kinetic study of Fluoride adsorption on Fe–Ag MBON, six initial Fluoride concentration was used in optimized conditions at room temperature, and the contact time was from 0 min to 60 min. For the equilibrium adsorption isotherm study of Fluoride adsorption on synthesized adsorbent, the initial Fluoride concentration ranged from 5 to 30 mg/L and other parameters have been set at optimum condition. Thermodynamic studies as well as carried out in optimized conditions at temperature ranged 293 to 323 °K.

2.5. Desorption Experiments

Six cycles of sorption and desorption were performed to examine the reusability of the Fe-Ag MBON. For sorption experiment, 500 mg of Fe–Ag MBON as sorbent was added into 1 L Fluoride solution of 10 mg/ L. The solution was stirred for 1 day at 200 RPM and room temperature. The pH of the solution was set in the neutral range during the sorption process. For desorption tests, the Fe–Ag MBON adsorbing Fluoride were dispersed in 100 ml NaOH 0.1 M solution. The blend was stirred for 1 h, then the sorbents were separated from NaOH solution and washed several times with DI-water and used for next cycle of adsorption–desorption. Follows formula was used for calculating the desorption percentage:

$$\text{Desorption (\%)} = \frac{\text{Desorbed Fluoride (mg)}}{\text{Adsorbed Fluoride (mg)}} \quad (3)$$

2.6. Effects of co-existing anions in experiments

The interfere effect of common coexisting ions such as Cl^- , PO_4^{3-} , HCO_3^- , SO_4^{2-} and NO_3^- on the Fluoride sorption were investigated by adding the salt of mentioned anions. The solution pH was adjusted in the neutral range. 500 mg of Fe–Ag MBON was added in each of the Erlenmeyer flask containing 50 ml fluoride solution of 10 mg/L and were mixed in 200 RPM for 1 day at room temperature. After separation the sorbent by magnet the residual Fluoride was analyzed.

3. Results and discussion

3.1. Surface morphology of Fe–Ag MBON

The morphology of Fe–Ag MBON before and after adsorption are respectively shown in Fig. 1. As shown in Fig. 1a, the pure iron oxide was aggregates formed compactly by ball-like nanoparticles of 10–25 nm while, Fig. 1e shows that the pure Ag oxide was aggregates of nanoflakes of 5–20 nm. Fig. 1b, c and d show that with increasing Fe/Ag ratio the size of Fe–Ag MBON decreased and their structures became firmer. Furthermore, by comparing Fig. 1f with another one can be found that the surface of adsorbent before sorption process have highly porous structure which was useful for achieving appropriate adsorption efficiency whereas the porous adsorbent surface changed significantly after the adsorption process, that indicated that fluoride ion was adsorbed into the pores of Fe–Ag MBON and developed a layer of on its surface.[30].

3.2. Specific surface area of Fe–Ag MBON

The N_2 adsorption and desorption isotherms of Fe–Ag MBON were shown in Fig. 2. The N_2 gas adsorption and desorption isotherms bass on the International Union of Pure and Applied Chemistry classification indicated that Fe–Ag MBON at a ratio of 3:1 is placed in type I while the other ratio of Fe–Ag MBON are type IV. Fe–Ag with 3:1 molar ratio was micro porous (average pore diameters <2 nm) and other materials with different molar ratio were mesoporous (2nm <average pore diameters> 50 nm) since they showed a hysteresis loop for the desorption isotherm.

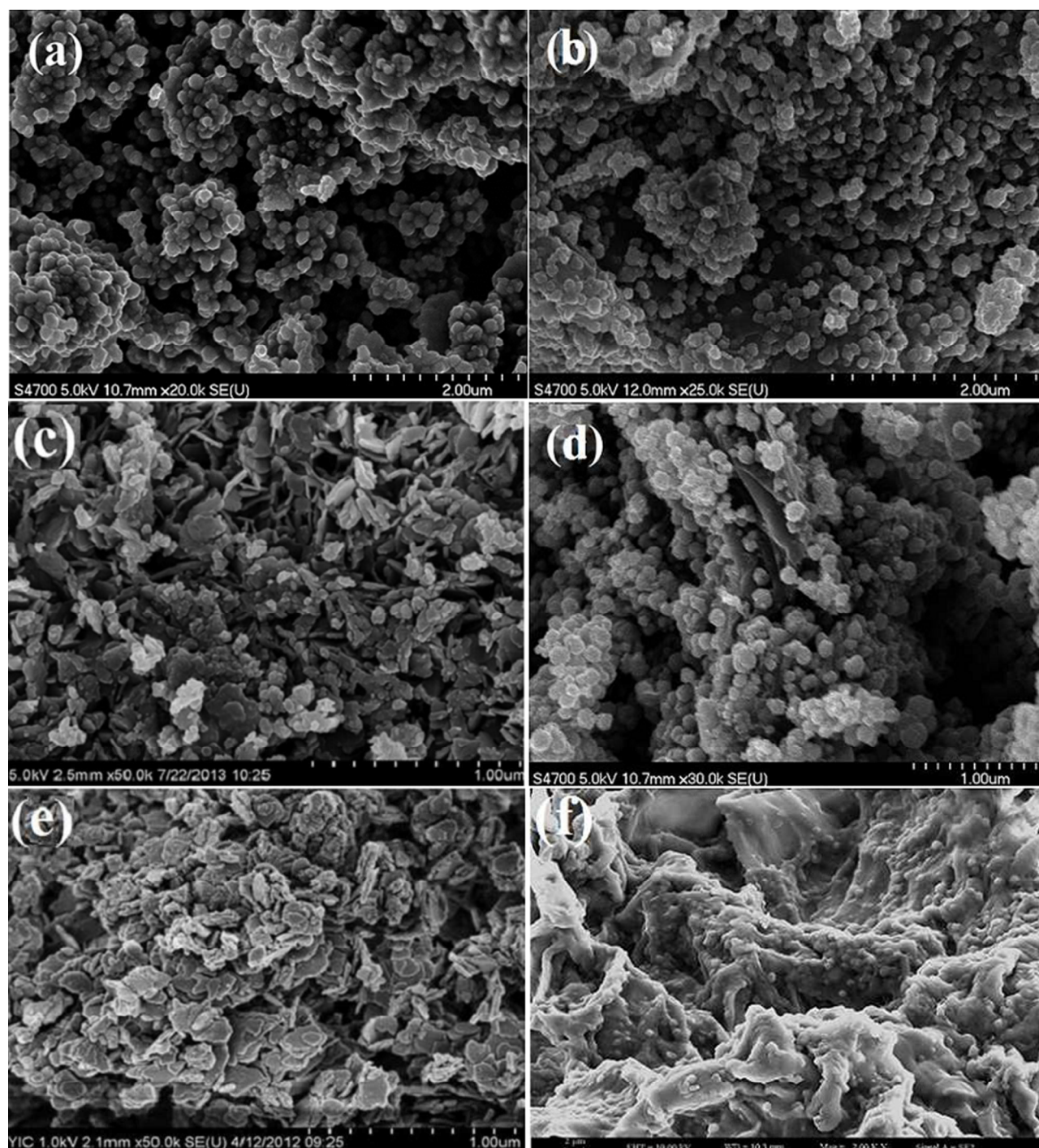


Fig. 1. SEM micrographs of Fe-Ag MBON. (a) Iron oxide, (b) Fe/Ag 3:1, (c) Fe/Ag 1:1, (d) Fe/Ag 1:3, (e) Silver oxide and (f) Fe/Ag 3:1 after Fluoride adsorption

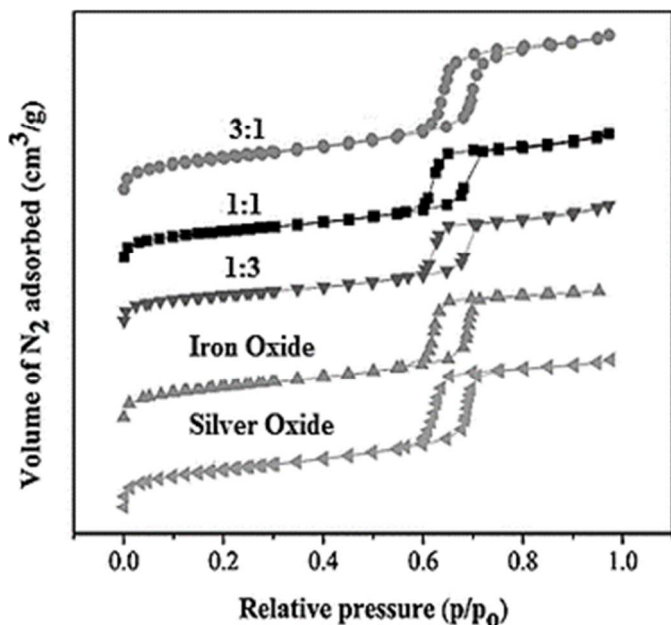


Fig. 2. N_2 adsorption/desorption isotherms of the Fe–Ag MBON with different molar ratios.

The specific surface area, average pore diameter, and average pore volume of Fe–Ag MBON were analyzed and their results summarized in Table.1.

Table 1. BET analyze, total pore volume and average pore diameter of the Fe–Ag MBON

Sorbent	BET area (m^2/g)	total pore volume (cm^3/gr)	Average pore diameter (Å)
Iron Oxide	94.96	0.252	5.84
3:1	254.24	0.678	1.31
1:1	189.57	0.391	6.91
1:3	145.74	0.479	6.21
Silver Oxide	74.34	0.224	4.21

It can be seen increasing in Ag content have a negative effect on the specific surface area of Fe–Ag MBON and led to its decrease, however, increased the pore diameter and the pore volume. For example, the surface area of Fe–Ag MBON 3:1 was over $254.24 m^2/g$, while the specific surface area of pure Ag and alone Fe oxide nanoparticles were determined at $94.96 m^2/g$ and $74.34 m^2/g$, respectively. This increase might be attribute to reduce of particle size and change in shape of the particle from nano fragment to ball-like nanoparticle in the binary nano oxide. In simpler terms, can be expressed that adsorbents with ball-like nanoparticle has the largest specific surface area compare than nano fragment materials [25]. Some researcher believed the replacement of Fe^{2+} with Ag^+ to form Fe–Ag solid solutions due to induce crystal defects could causing the promotion of their specific surface areas. This further illustrates that these samples were not simple mixtures of FeO and Ag_2O nanoparticles and a noteworthy synergistic effect existed in this binary oxide system. Among Fe–Ag MBON with different molar ratio, $Fe_{0.75}Ag_{0.25}O_2$ (3:1) nanoparticles with $254.24 m^2/g$ have largest specific surface area which may be attributed to the smallest crystallite size of them. Largest specific surface along with highest total pore volume ($0.678 cm^3/g$) and

average pore diameter 8.31 nm has led that $\text{Fe}_{0.75}\text{Ag}_{0.25} \text{O}_2$ converted to the adsorbent with well adsorption performance.

3.3. Energy dispersive X-ray of Fe–Ag MBON

The EDX spectrum of Fe–Ag MBON before and after adsorption process are recorded in Fig. 3. The element peaks of O and Ag were observed at the energy values of 0.5 keV, 3 keV, and energy values of 1.25 and 6.6 keV attributed to Fe (Fig. 3a), this indicates that Fe and Ag were successfully synthesized. Moreover, the adsorption of Fluoride on the surface of Fe–Ag MBON was ascertained from the EDX spectrum which shows the presence of Fluorine along with the other major peaks.

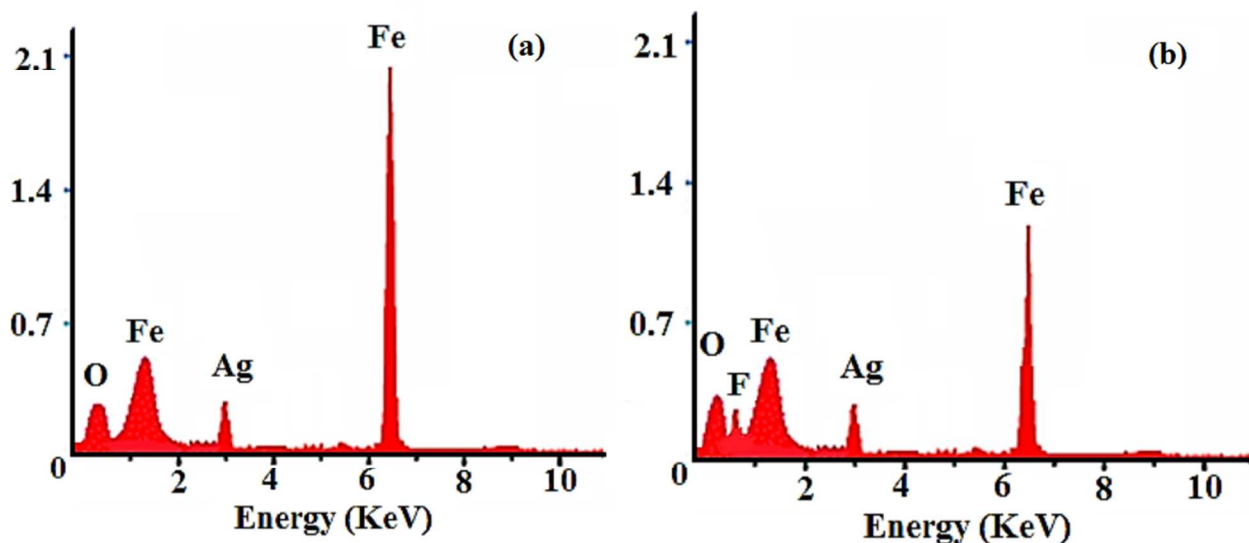


Fig.3. EDX spectra of Fe–Ag MBON (a), before and (b) after adsorption process

3.4. X-ray diffraction spectroscopy of Fe–Ag MBON

Fig. 4 (a) shows the XRD patterns of Fe oxide (Fe_3O_4) nanoparticles with no silver component existed. XRD diffraction peaks appeared at 2θ of 35.4° and 77.2° which corresponds to (110) and (211) Bragg reflection respectively, in accordance with the typical XRD diffraction peaks of Fe_3O_4 cubic fluorite structure based on PDF 34-0394[31, 32]. Fig. 4 (b) present the silver oxide nanoparticles in the absence of Fe_3O_4 nanoparticles component. XRD diffraction peaks appeared at 2θ of 37.8° , 64.7° and 73.9° attributable to the indices (111), (220) and (311) indicates existence of Ag[33] and in consistent with the typical XRD diffraction peaks of Ag_2O tetragonal phase based on PDF 49-1642. These peaks were also observed in the pattern of synthesized Fe–Ag MBON, indicating that the cubic phase of Fe_3O_4 is maintained after Ag loading. (Can see in Fig. 4 (c))

The Scherrer's formula applied to the calculated crystallite size of Fe–Ag MBON from the strongest XRD peak and the results presented in Fig 4 (d)

$$D = 0.9\lambda/\beta\cos\theta$$

Where: D (nm): mean size of the crystalline domains, λ : the average X-ray wavelength, β : the line broadening at half the maximum intensity, θ : the Bragg angle.

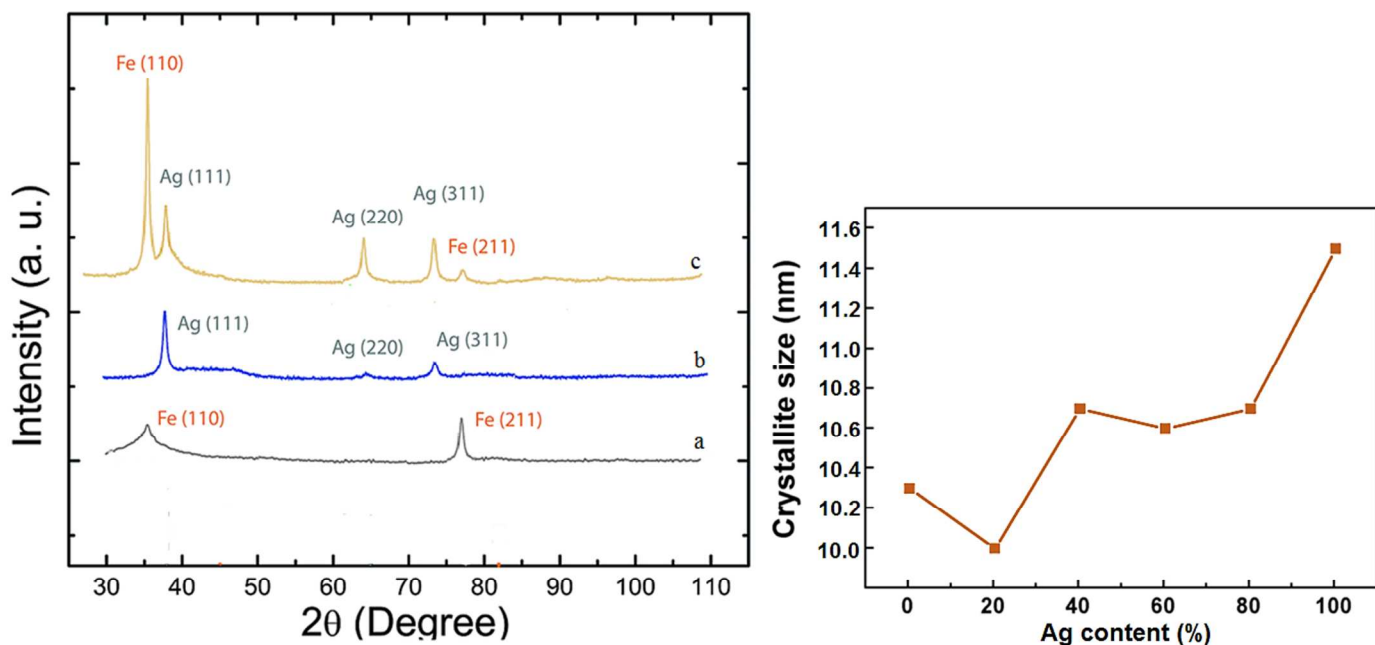


Fig.4. X-ray diffraction patterns of (a) Fe, (b) Ag and (c) Fe–Ag MBON in ranges of $2\theta = 30 - 110$ by using $\text{Cu } \alpha$ radiation, (d) crystallite sizes of Fe–Ag MBON with the changes in amount of Ag content

With the increase of silver content to 20 %, the crystallite size decreased slightly from ~ 10.25 nm to ~ 9.8 nm, however, with the further increase of the silver content from 20 to 100 %, the observed that the particle size began to increase from ~ 9.8 nm to ~ 11.47 nm. The replacement of heavier Ag^+ by lighter Fe^{2+} in $\text{Fe}_{0.75}\text{Ag}_{0.25}\text{O}_2$ could induce crystal defects and cause reduces the size of the nanoparticles degree. According to the evidence can be found that with increasing the replacement/substitution rate of $\text{Ag}^+ : \text{Fe}^{2+}$ the size of nanoparticles began to decrease.

3.5. Dynamic light scattering and transmission electron microscopy of Fe–Ag MBON

Structure and shape of Fe–Ag MBON was analyzed by TEM micrographs at 90 keV (Fig.5a). According this analysis, synthesized absorbent were sphere shaped structure, almost uniform and intertwined.[34]. DLS results are depicted in Fig.5b. DLS curves strongly indicate the small Ag NPs (~ 5 nm) distributed on the Fe (~ 10 nm) surface which well accordance with the TEM finding.

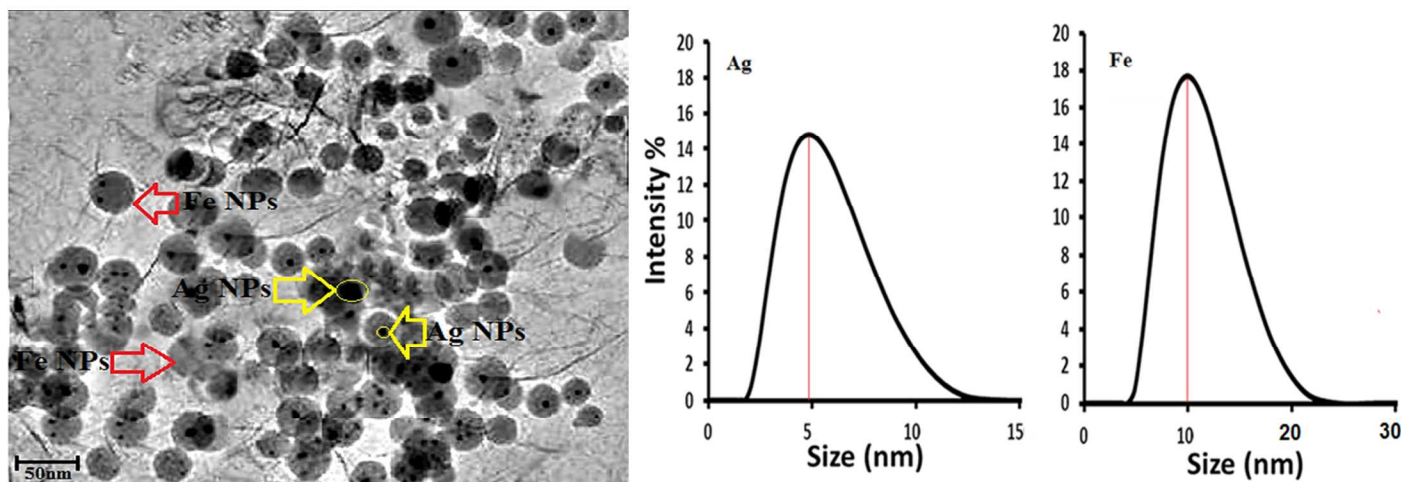


Fig.5. TEM images of Fe–Ag MBON (a) DLS curve of Fe, and Ag (b)

3.6. Vibrating sample magnetometer

For determining the magnetic properties of Fe–Ag MBON, VSM analysis was performed in magnetic field of ± 100 kOe at 25 °C. VSM curve showed the maximum saturation magnetization for Fe–Ag MBON was equal to 80 emu/g. The achieved results depict that Fe–Ag MBON is superparamagnetic and can easily separate from samples by an external magnetic field without secondary pollution (Fig.6).

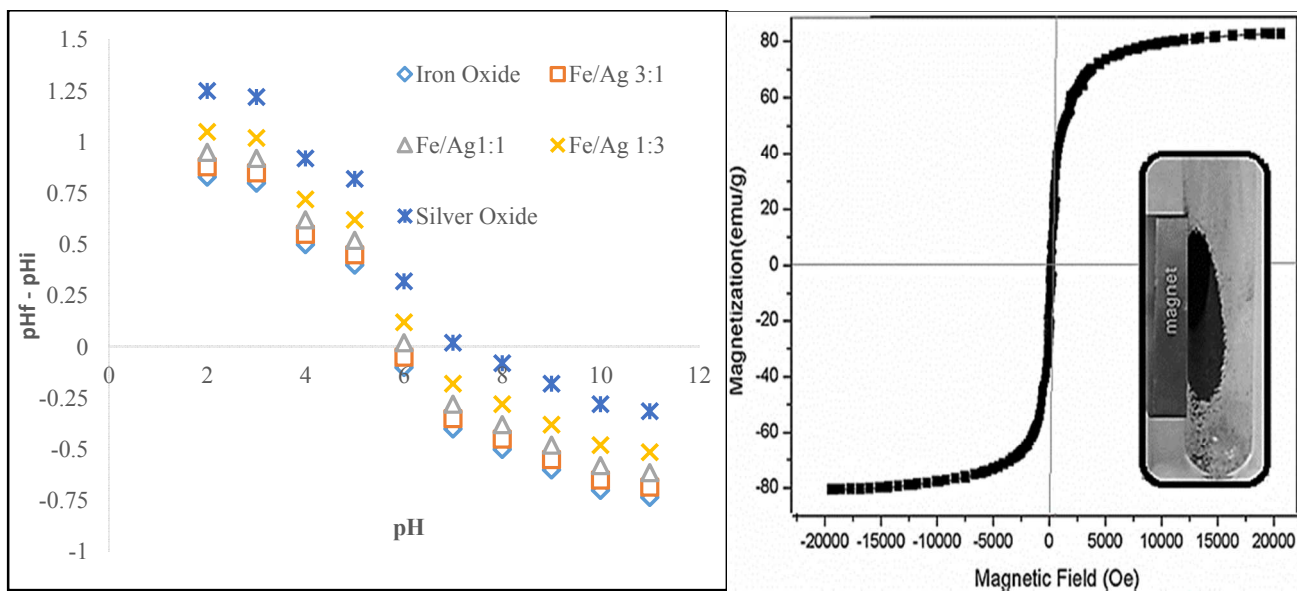


Fig.6. VSM analysis of Fe–Ag MBON and magnetic separation of it from aqueous solution (insert) (a) Points of zero charge (pzc) determination for Fe–Ag MBON (b)

3.7. Point of zero charge (pzc)

The pzc values of Fe–Ag MBON were shown in Fig. 6b. The pzc of iron oxide, Fe/Ag 3:1, Fe/Ag 1:1, Fe/Ag 1:3 and silver oxide were 5.91, 6.03, 6.7, 6.1 and 7.1, respectively. Clearly, the pzc value raised as Ag content increased in these oxides.

3.8. Effect of Ag loading on removal efficiency

The effect of the Fe^{2+} , Ag^+ , Fe_3O_4 , Ag_2O and Fe–Ag with various molar ratios (3:1, 1:1, and 1:3) on the removal efficiency is shown in Fig. 7. The Fe–Ag adsorbent reached the highest adsorption capacity of 20.61 mg/g, which was much higher than of other samples, at the Fe–Ag ratio of 3:1. These results completely comply with the results of BET analyze and showed the synergistic effect of Fe and Ag on fluoride adsorption capacity at a molar ratio of 3:1.

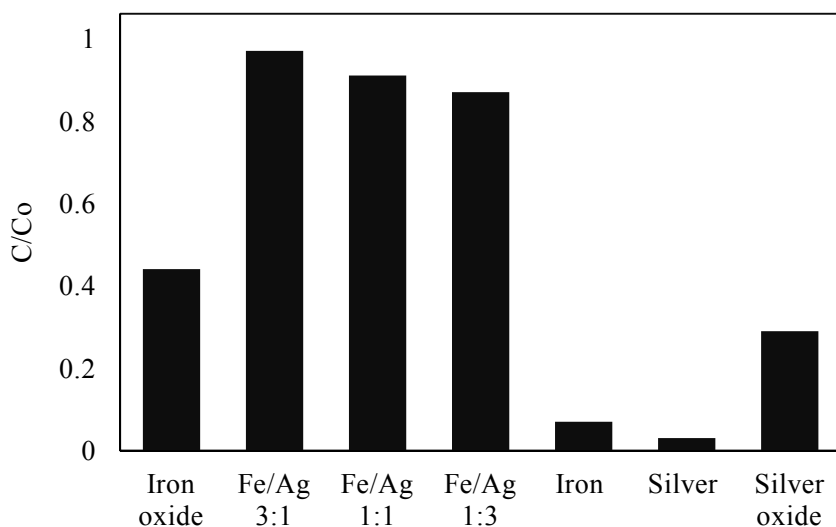


Fig.7. effect of the Fe^{2+} , Ag^+ , Fe_3O_4 , Ag_2O and Fe–Ag MBON on removal efficiency

3.9. Solution pH Effect on Fluoride Adsorption by Fe–Ag MBON

The solution pH is a significant factor that effects on defluorination at the solid/liquid interface. This parameter by changing the surface charges and functional groups can influence on the surface properties and active sites of the sorbents. Fluoride removal by different pH as a function of time were studied and the results shown in Fig 8a.

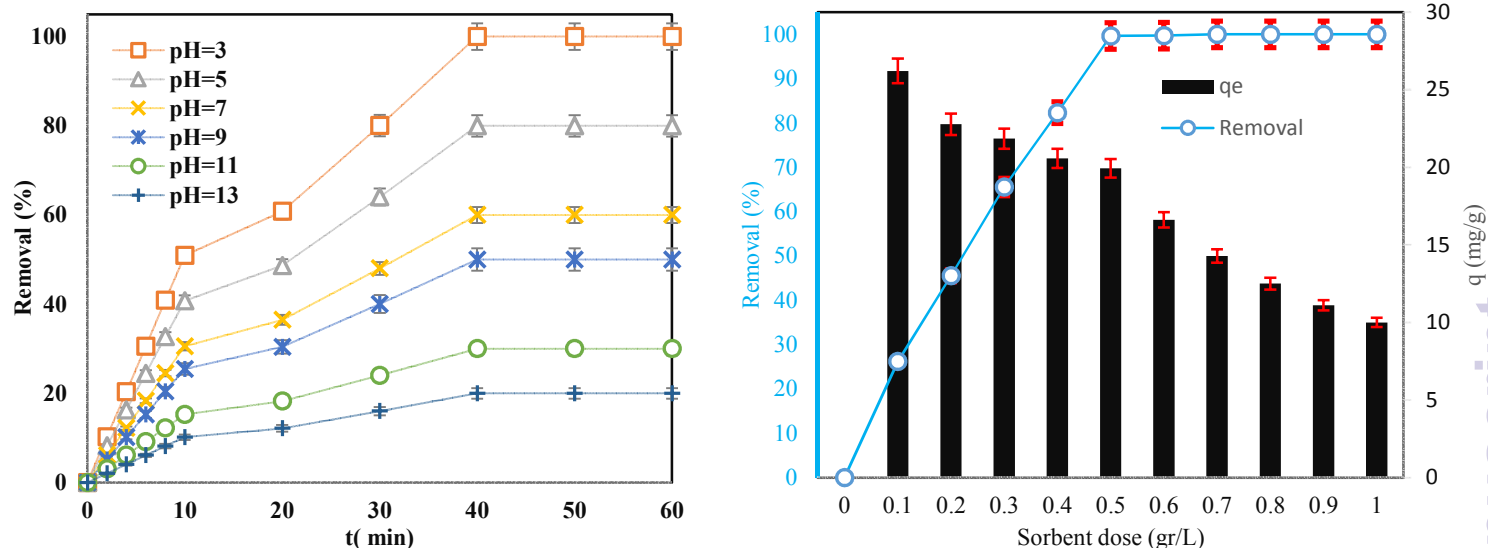
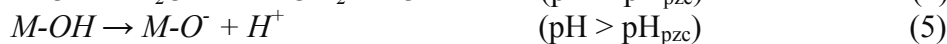


Fig .8. (a) Effects of solution pH on defluorination by Fe–Ag MBON. Initial fluoride concentration: 10 mg/ L, adsorbent dose: 200 mg/L at room Temperature. (b) Effects adsorbent dose on Fluoride removal

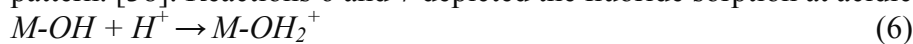
Fig. 8 (a) shows clearly that Fluoride adsorption on Fe–Ag MBON was pH-dependent. Under the acidic pH (pH = 3), the adsorption performance increased to 100%, while it dropped much faster at neutral and basic condition. These results may be the following reason that in acidic pH, increase the productions of positive protons (H^+) that can be dominated the surface of Fe–Ag MBON cause induced a positive charge on the adsorbent surface. Thus electrostatic gravity force between the positive protons attached on surface of Fe–Ag and negative molecules of Fluoride lead to increase of adsorption capacity.[35] The decrease Fluoride adsorption in alkalinity pH, is due to elevated of hydroxide ions production. The electrostatic repulsion force between OH^- ions (Hydroxide) and negative charges of Fluoride prevent the diffusion of Fluoride ions and caused a decrease of adsorption capacity. Since that maximum efficiency of Fluoride removal was occurred at pH=3, this pH chosen for future experiment. Similar phenomena reported by other researchers in F^- adsorption by various binary oxides [36, 37]. In other hand, the surface charge of Fe–Ag MBON is related to the pH_{ZPC} and pH of the solution. When $pH > pH_{pzc}$, the surface charge is negative and with getting bigger pH pzc compare pH, positive charge induced on surface of sorbent.

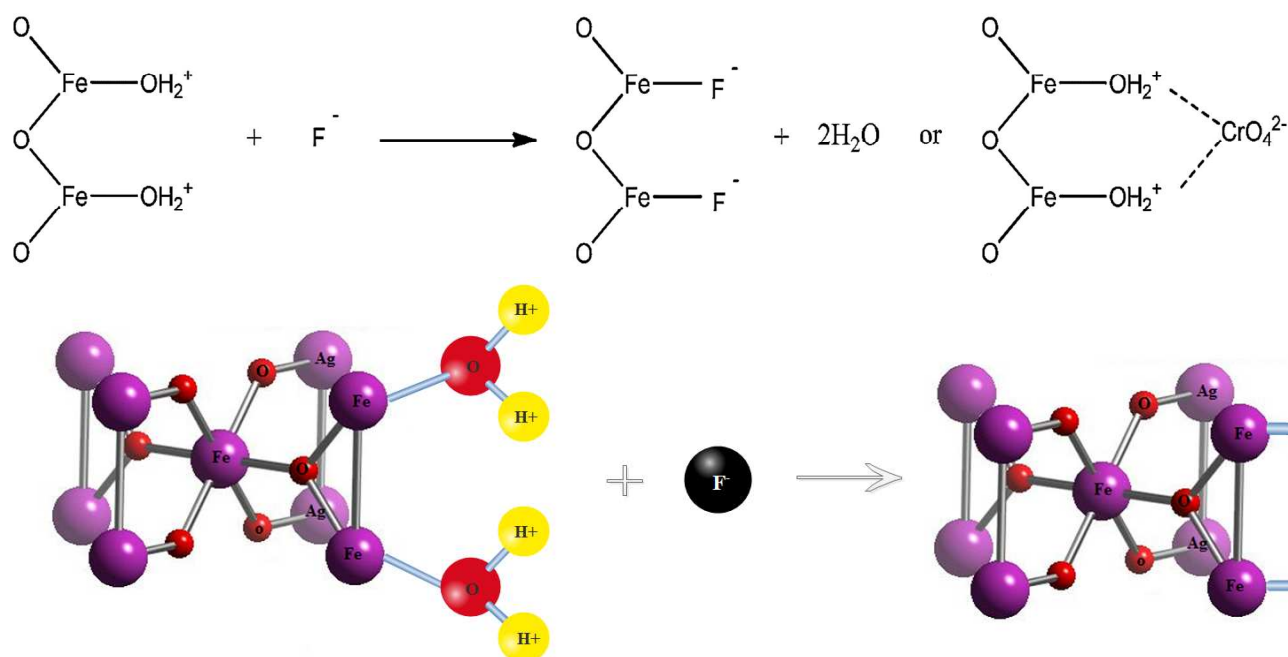


Where, M indicates metal ions like Fe^{2+} , Ag

In this work the point zero charge (pH_{PZC}) calculated for the synthesized Fe–Ag MBON and depicted in Fig. 6a. The results showed pH_{PZC} for our sorbent was 5.6 and the best defluorination was achieved at pH equal 5.

So it could be concluded, at $pH < 5.6$ the surface of the adsorbent has positively charged which confirms the above contents. In addition base on the significant relationship between pH and pH_{pzc} it could be concluded that the mechanism of fluoride adsorption followed a non-specific adsorption pattern. [38]. Reactions 6 and 7 depicted the fluoride sorption at acidic condition:





Scheme 1. Effects of solution pH on defluorination by Fe–Ag MBON.

3.10. Influence of adsorbent dose on Fluoride removal

Adsorbent dose appears to have an important influence on adsorption capacity and removal efficiency. Adsorption of 10 mg/L Fluoride concentration by different sorbent dosages (0.1-1 gr/L) were studied at room temperature. Fig.8b shows that with increase of adsorbent dosage from 0.1 to 1 g/L, the removal percentage increased from 26.21% to 100% and adsorption capacity (q) decreased from 26.21 to 10 mg/g. It is explained that with increase the amount of sorbent provides greater number of surface area (available active sites) for the Fluoride binding [39]. Wei Ma et al in study of Fluoride removal by Mg–Al–Fe hydrotalcite-like compound reported with increased adsorbent dosage from 0.1 g/L to 2g/L removal efficiency is increased from 40% to 85%. [40]. In the present work the highest efficiency of Fluoride adsorption achieved to 1 gr/L adsorbent, however, with considering the creating adsorbent cost and worthless effect of Fluoride removal with increasing sorbent from 0.5 to 1 g/L, using 0.5 gr/L adsorbent will be economical. Therefore, 0.5 gr/L adsorbent dosage was chosen to future the experiment.

3.11. Effect of contact time and kinetics equilibrium studies

The kinetics of the Fluoride adsorption from aqueous solutions onto Fe–Ag MBON with Five initial fluoride concentrations (5, 10, 15, 20, 25 and 30 mg/L), at the optimized condition was examined and the results presented in Fig 9. This figure shows in all concentration most Fluoride adsorption and highest rate of defluorination occurred within the first 20 min of contact. For example, 100% Fluoride was removed after 20 min when the initial Fluoride concentration was less than 10 mg/L. The observed rapid defluorination could be attributed to below reasons:

- i. The existing many vacant adsorption sites in adsorbent surface in initial time, which is filled with time passed

- ii. Fe–Ag MBON have a nano size, thus, the distance of Fluoride for diffusion from the bulk solution onto active sites is shortened
- iii. Prepared sorbent in Nano scale cause large external surface area and proper pore size/volume which provided well contact efficiency with Fluoride

When the initial Fluoride concentration increased to 15, 20, 25 and 30 mg/L, Fluoride removal decrease to about 84.1%, 60%, 50.2% and 30.3% after 20 min, respectively. Fixed vacant adsorption sites versus increasing concentrations of contaminants is reason of relatively lower Fluoride removal ratio, while with increasing the initial Fluoride concentration from 5 to 30 mg/L, adsorbed Fluoride amount increased from 10.0 mg/g to 18.9 mg/g. It is notable that vacant adsorption sites and external surface area with further increase of the adsorption time filling and be caused adsorption rate slowed down and gradually reached the equilibrium state. Adsorption of Fluoride from aqueous solution using meso-structured zirconium phosphate was studied by Swain (2011) and confirm these results. Swain reported with past the time active site which can F⁻ sorption would be filled and removal efficiency will be reduced.[41].

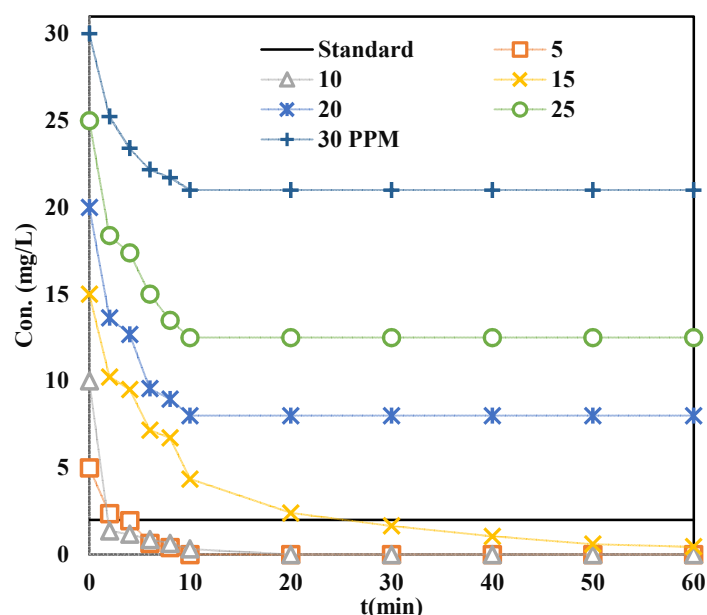


Fig 9. Effects of contact time on defluorination by Fe–Ag MBON. PH=3, adsorbent dose: 0.5 g/L and room Temperature

In the present study, we have been using pseudo-first-order and pseudo-second-order models to establish the best fitted model for experimental data and describe the kinetic behavior of Fluoride sorption on the Fe–Ag MBON. The pseudo-first and second order model equations are defined as:

$$\ln(q_e - q_t) = \ln q_e - K_1 t \quad (8)$$

$$\frac{t}{qt} = \frac{1}{K_2 q_e^2} + \frac{1}{q_e} t \quad (9)$$

Where, q_e (mg/g): adsorption capacity of the sorbent in equilibrium time, q_t (mg/g) : adsorption capacity of the adsorbent at time, K_1 (L/min): coefficients of reaction rate for the pseudo-first-order models, K_2 (mg/g.min): coefficients of reaction rate for the pseudo-second-order models. The related parameters of pseudo-first and second order kinetic can be calculated from the plots $\log q_e - q_t$ and qt/t versus t , respectively. The regression coefficient (R^2) and compatibility between q_e

(experiment) with q_e (calculate) used to choose the best kinetic models. The fitting curves of the Fluoride adsorption kinetic data presented in Fig.10 and their parameter values are given in Table 2. The results showed the pseudo-second-order model with $R^2 > 0.968$ in all concentration can be better described adsorption of Fluoride, that exhibits the rate-limiting is chemisorption and sharing of electrons from sorbent and adsorbate involving covalent forces. [23] In addition $q_{e,cal}$ at the pseudo-second-order compared to other models were more closer with $q_{e,exp}$. In a similar study, Swain et al illustrated that the pseudo-second order model with $R^2 = 0.95$ describe better the kinetics of fluoride sorption on alginate entrapped Fe(III)–Zr(IV) binary[23]. This findings is same with the results reported for the Fluoride sorption on trimetal-oxide adsorbent[4], nano zirconium chitosan composite[42] and composite material of biopolymer alginate entrapped mixed metal oxide nanomaterials [43]

Table 2. Pseudo-second-order kinetic and pseudo-first order model parameters for binary metal oxide

models	parameters	Concentration (mg/L)				
		10	15	20	25	30
pseudo-first order	$q_{e,cal}(mg/g)$	21.6	27.9	32.3	41.8	46.3
	$K_1(min^{-1})$	0.137	0.123	0.119	0.103	0.089
	R^2	0.860	0.865	0.865	0.884	0.896
pseudo-second order	$q_{e,cal}(mg/g)$	23.61	36.54	41.27	52.3	58.91
	$k_2(g/mg)(min^{-1})$	4	4.35	5.56	5.84	6.01
	R^2	0.978	0.985	1	0.968	0.999
Experimental		20	21.54	24.27	26.3	28.69

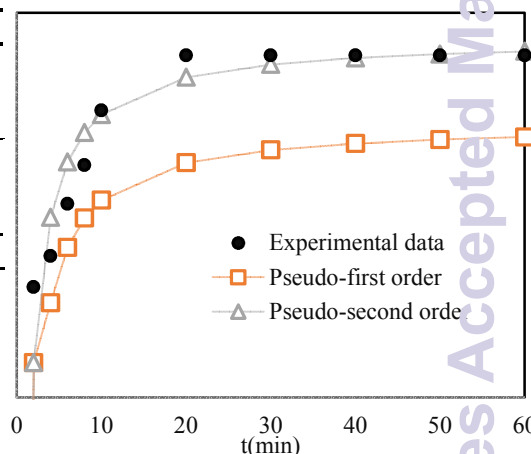


Fig 10. Kinetics of Fluoride removal by Fe–Ag MBON at pH 3 and 25 ± 1 °C

3.12. Adsorption isotherm studies

Analysis of the isotherms equilibrium is a vital stage in designing of the sorption systems. Langmuir, Freundlich, Temkin and Dubinin–Radushkevich models used to investigate the behavior of Fluoride sorption and determine the maximum adsorption capacity of Fe–Ag MBON at room temperatures in 10 mg/L initial concentration. Linear equations of isotherm models following from below formula:

$$q_e = k_F (C_e)^{1/n} \quad (10)$$

$$q_e = (q_m k_L C_e) / (1 + k_L C_e) \quad (11)$$

$$q_e = q_m \ln K_T + q_m \ln C_e \quad (12)$$

$$\ln q_e = \ln q_m - D \epsilon^2 \quad (13)$$

Where, K_F ((mg/g) (L/g)^{1/n}): Freundlich constant, $1/n$: Freundlich exponent, K_L (L/mg): Langmuir isotherm constant, K_T (L/mg): Temkin isotherm constant, D (mol² /kJ²): Dubinin–Radushkevich isotherm constant. The relative parameters of Langmuir, Freundlich, Temkin and Dubinin–

Radushkevich isotherm models were calculated from the plots between $[Ce/q_e \text{ vs. } Ce]$, $[\log(q_e) \text{ vs. } \log(Ce)]$, $[q_e \text{ vs. } \log(Ce)]$ and $[\ln q_e \text{ vs. } \epsilon^2]$. Fig.11 presents the isotherms resulted of the Fluoride adsorption onto Fe-Ag MBON. Furthermore, Table 3 reports the other isothermal parameters obtained in fitting the experimental data. As shown in Table 3, the Langmuir model with $R^2 > 0.976$ have a higher regression coefficient compare than other models, so, this model is very well fitting for describe the sorption behavior of Fluoride on Fe-Ag MBON. Similar findings were reported in the literature about the removal of Fluoride by different types of adsorbents [44, 45]. The Langmuir adsorption capacity (q_{max}) was determined at 20.57 mg/g at 298 °K. Table.4 summarizes the reported q_{max} of other binary oxide on Fluoride in literature, compared with prepared Fe–Ag MBON in our study. It was found that the adsorption capacity of Fe–Ag MBON was premiered to many other adsorbents. It may be due to increase of the porous structure in the adsorbents. It was about 27 % higher than Fe-Zr binary oxide while it was 55 % Lower than Fe-Mn binary oxide in aqueous environment. Therefore, synthesized adsorbent could be considered as a new adsorbent for removal of fluoride.

Table 3. Langmuir, Freundlich, Dubinin–Radushkevich and Temkin isotherm constants for fluoride adsorption by Fe-Ag MBON.

models	parameters	Linear method	Non- Linear method
Langmuir	q_m (mg/g)	20.91	21.57
	k_L (L/mg)	1.38	1.41
	R^2	0.976	0.998
	R_L	0.2	0.31
Freundlich	k_f (mg/g(L/mg) ^{1/n})	19.87	18.96
	n	15.82	15.53
	R^2	0.911	0.931
Temkin	K_t (mg/g(L/mg) ^{1/n})	13.79	14.12
	b_t	210.06	211.45
	R^2	0.903	0.903
D-R	q (mol/g)	1.14×10^{-5}	1.17×10^{-5}
	D (mol ² /kJ ²)	0.0047	0.0049
	E (kJ/mol)	14.89	13.93
	R^2	0.944	0.964

Table4. Comparison of various Binary oxides for fluoride removal

Adsorbent	Solution pH	Max sorption capacity (mg.g-1)	Ref.
Fe-Ag (25 °C)	5	20.57	This work
Fe-Mn	5.6	79.5	[46]
Fe-Zr	4	13.6	[23]
Al-Zr	5	5.8	[47]
Fe-Ti	ND	27.5	[24]
Ti-Al	3	2.22	[48]
Ce-Zr	5.8 ± 0.2	19.5	[49]

All the information implied that the Langmuir models could be suggested for Fluoride sorption by Fe—Ag MBON that refers to the adsorption process occur on homogeneous surface and Fluoride adsorption taken in a monolayer adsorption manner.

The R_L parameter is the dimensionless constant factor which indicates the affinity of adsorbed material to the adsorbent and calculated using Eq 14:

$$R_L = \frac{1}{1 + K_L C_e} \quad (14)$$

Based on R_L factor the nature of the isotherm to be classified as follows:

$R_L > 1$: unfavorable isotherm;

$R_L = 1$: linear isotherm;

$0 < R_L < 1$: favorable isotherm;

$R_L < 1$: irreversible isotherm.

The R_L value in this experiment is between 0 and 1 that indicate the Fluoride molecules are desirably adsorbed on adsorbent.

Some literature used from Dubinin-Radushkevich isotherm to obtain the mean energy of adsorption as given in Eq:

$$E = 1/(2D)^{0.5} \quad (15)$$

Chemisorption process happened when $8 < E < 16$ kJ/mol, while in $E < 8$ kJ/mol physical adsorption process occurred. In present study E value was determined at 14.89 kJ/mol, thus, the Fluoride adsorption onto Fe–Ag MBON was a chemisorption process.

3.13. Effect of temperature and thermodynamic study of Fluoride removal

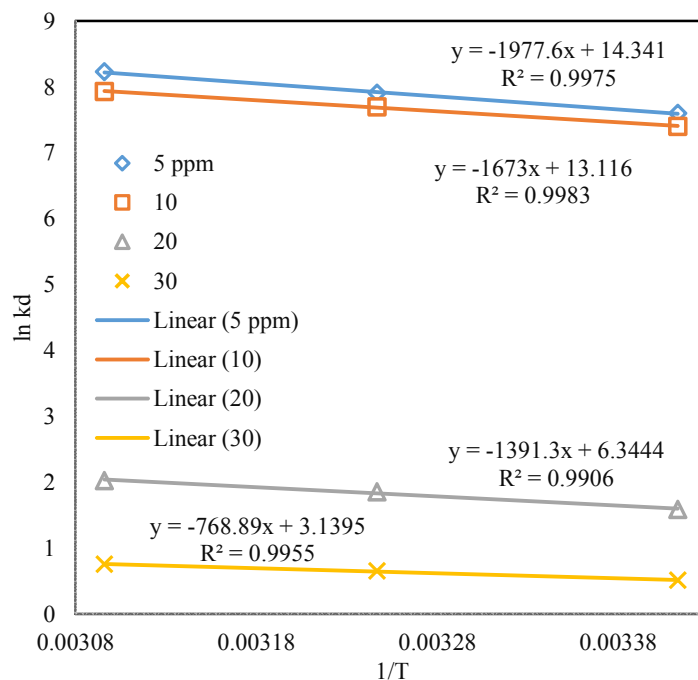
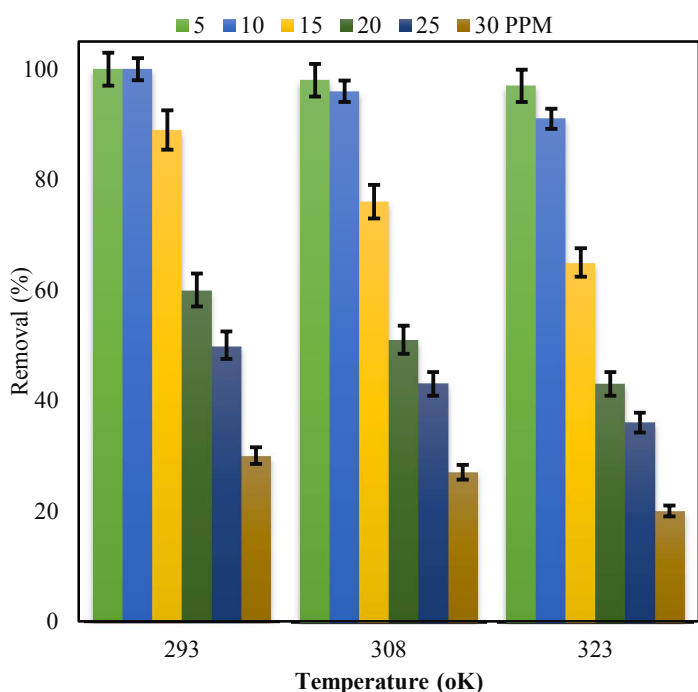


Fig .12. Effect of temperature on the adsorption of fluoride onto Fe–Ag MBON (PH=3, adsorbent dose: 0.5 g/L, and contact time 20 min (a) Van't Hoff curve

To determine the impact of the temperature on the Fluoride adsorption at various initial concentrations, temperature varied from 293 to 323 °K while the contact time was selected as 20

min. The result revealed that increasing the temperature had a negative effect on the adsorption process (Fig.12) and lower temperature is favored to removal of fluoride.

Table 5. Thermodynamic parameters for Fluoride adsorption by Fe-Ag MBON

<i>Con. (mg/l)</i>	<i>Temperature(oK)</i>	<i>lnk_d</i>	<i>ΔG⁰(kJ/mol)</i>	<i>ΔH⁰(kJ/mol)</i>	<i>ΔS⁰(kJ/mol.K)</i>
5	293	7.60	-18.51	-237.86	0.12
	308	7.90	-20.23		
	323	8.22	-22.10		
10	293	7.40	-18.03	-201.23	0.11
	308	7.70	-19.71		
	323	7.93	-21.29		
20	293	1.58	-3.86	-167.34	0.053
	308	1.85	-4.72		
	323	2.02	-5.43		
30	293	0.51	-1.24	-92.48	0.026
	308	0.65	-1.67		
	323	0.75	-2.02		

The distribution coefficient constant (K_d) used for determining the thermodynamic values and the slope and intercept of the Van't Hoff plot ($\ln K_d$ versus $1/T$) are used for calculating the numerical values of ΔH^0 (the change in the enthalpy (Kj/mol)) and ΔS^0 (the amount of energy change (J/mol K)), respectively which defined as:

$$\ln k_c = \frac{\Delta S^0}{R} - \frac{\Delta H^0}{RT} \quad (16)$$

$$\Delta G^0 = \Delta H^0 - (T\Delta S^0) \quad (17)$$

Where: K_d is the distribution coefficient (L/g), R is the universal gas constant (8.314 J/mol.K) and T is solution temperature ($^{\circ}$ K). The Van't Hoff graph were shown in Fig. 12b and the Fluoride adsorption thermodynamic parameters on Fe–Ag MBON are represented in Table 5. A negative values in standard free energy acquired in our studies exhibits that the sorption process is a spontaneous reaction. The value of ΔH^0 is negative that confirms the adsorption process is exothermic in nature. The value of ΔS^0 was found from 0.026 to 0.12, which indicated that the randomness increased in solid /liquid interface during the Fluoride sorption process with increasing temperature.

3.14. Coexisting anions effect on fluoride adsorption by Fe-Ag MBON

Foreign anions such as SO_4^{2-} , NO_3^- , Cl^- , HCO_3^- and PO_4^{3-} usually presence in drinking water that can compete with Fluoride for the available sites. So the impact of mention ions as competing parameter on defluorination were examined. In order to evaluate the effect of co-existing anions, fluoride concentration was kept at 10 mg/ L and initial concentration of co-ions with dissolved of their sodium salts were studied from 0 to 130 mg/L. Fig. 13a can be shown that NO_3^- , Cl^- , SO_4^{2-}

have a slight effect on defluorination processes. However, the presence of PO_4^{3-} and HCO_3^- have a significantly impact on defluorination processes. As can be seen in Fig. 13a, the Fluoride sorption efficiency decreased approximately 30 and 52% by increasing the PO_4^{3-} and HCO_3^- ions respectively to 120 mg/ L. Generally would be expected that PO_4^{3-} and HCO_3^- to occupy the active adsorption site have a high interest to compete with Fluoride which will eventually lead to reduce the defluorination efficiency. Furthermore, the impact of studied anions towards sorption process may be due to their affinity towards the sorbent substance.

3.15. Fluoride desorption studies

Adsorption/desorption of Fluoride by Fe–Ag MBON were performed in batch condition and shown in Fig.13b. Mention figure shows that reusability of Fe–Ag MBON slightly reduced after the six successive sorption–desorption cycles. So we suggested that Fe–Ag MBON can be repeatedly used for Fluoride sorption without many losses in initial sorption efficiency. Furthermore, > 62.81% adsorbed Fluoride could be desorbed/recovered in the presence of NaOH in the sixth cycle which can be used in different cases like industrial applications.

To test whether Fe and Ag leach out into the solution from the Fe–Ag MBON surface, the samples were analyzed by applying ICP-MS after each reaction cycle. Based on the results, the residues of Fe and Ag were not detected. In previously conducted studies, it has been reported that relatively higher amount of the residues of Cu and Pd was detected during the removal of contaminants by bimetallic adsorbent and catalysts which were supported by activated carbon (18.1%)[50], carbon nanotube (15.9%) [51], silica oxide (10.6%), alumina (30.7%), and zirconium oxide (26.0%) [52, 53]. Considering the result of the present study, it can be speculated that Fe–Ag MBON has acceptable stability and durability to strongly bind the bimetals to each other; which can be regarded as an advantage for its recycling in continuous Fluoride removal.

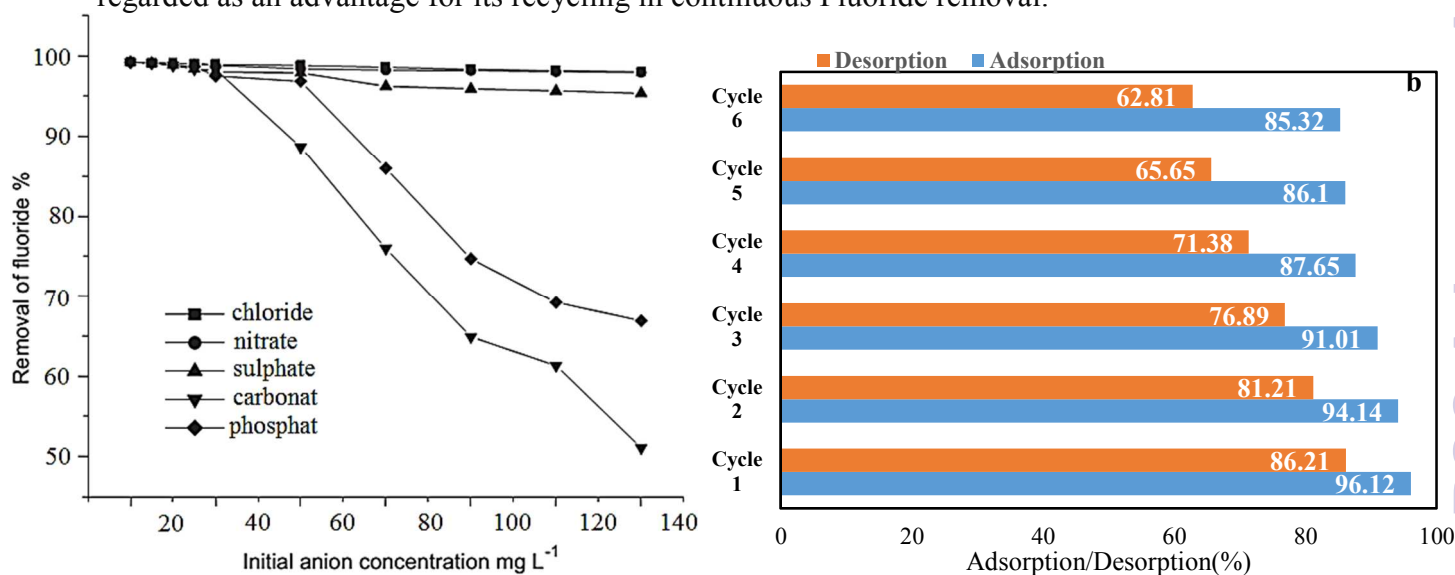
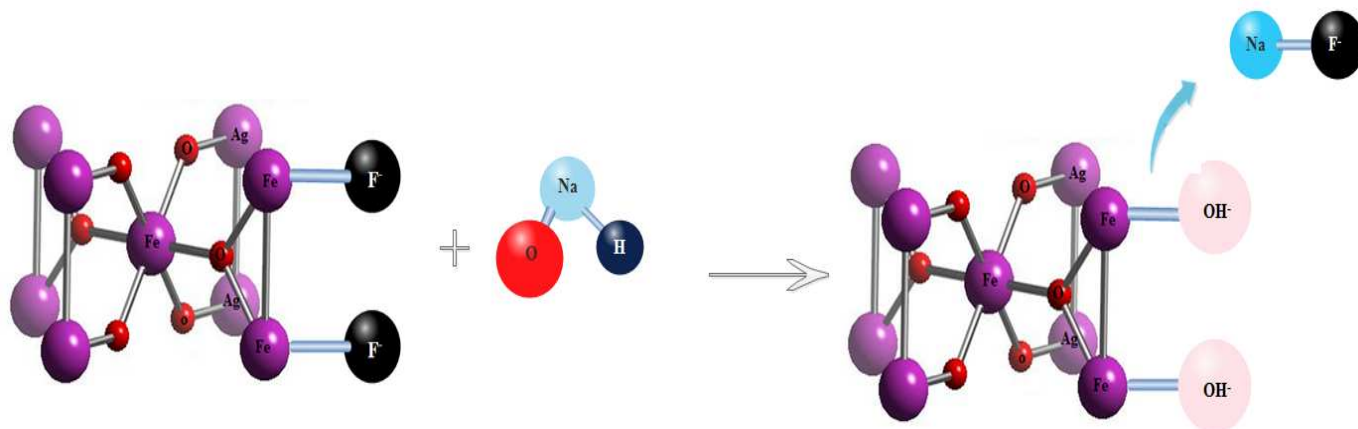


Fig. 13. Effect of co-anions on fluoride adsorption efficiency using Fe–Ag MBON (a), Adsorption /desorption of binary metal oxide (b)



Scheme 2. mechanism of Fluoride desorption on Fe–Ag MBON.

3.16. Mechanism of fluoride adsorption

The FTIR spectra of the Fe oxide, Ag oxide and Fe–Ag oxide before and after adsorption are revealed in Fig.14. For three samples, the created band at 3440 cm^{-1} was allocated to the carbonate adsorbed, it is because the sorption experiments were perform open to the atmosphere. The common peak in the Ag oxide and Fe–Ag MBON at 1398 cm^{-1} was apparent that not present of Fe oxide. In the FTIR spectra the peaks at near 1120 cm^{-1} in the all three oxides can be apportioned to the bending vibration of the hydroxyl (OH^-) of metal oxides (Metal–OH). It was discovered that tow peaks at 1398 and 1120 cm^{-1} can be regarded as the identify factors for the active sites of the adsorbents. The peak at 587.8 cm^{-1} was assigned to Fe oxide and created peak at 615.2 cm^{-1} assigned to Ag oxide. However, the Fe–Ag oxide had its distinctive peak at a wave number of 448.0 cm^{-1} , which was intelligibly lower than those of Fe and Ag oxide. From Fe oxide (blue curve) shifting in range of 1398 to 1120 cm^{-1} , it was deduced that Fe– O_2 –Ag bonds were formed in the Fe–Ag MBON adsorbent. Generally, with considering to morphologies, XRD and above analysis can be inferred which Fe and Ag have a synergistic effect on the structure of Fe–Ag MBON and was not a simple combination between Ag oxide and Fe oxide. After Fluoride adsorption clearly observed that large changes happened on the FTIR spectrum of Fe–Ag MBON. Vibration peaks near 1120 cm^{-1} (Metal–OH) got largely weakened that implied the loss and decrease of surface hydroxyl groups during the Fluoride uptake. In other word, surface hydroxyl groups (M–OH) were replaced by the adsorbed Fluoride and can play an important role in the adsorption of Fluoride.

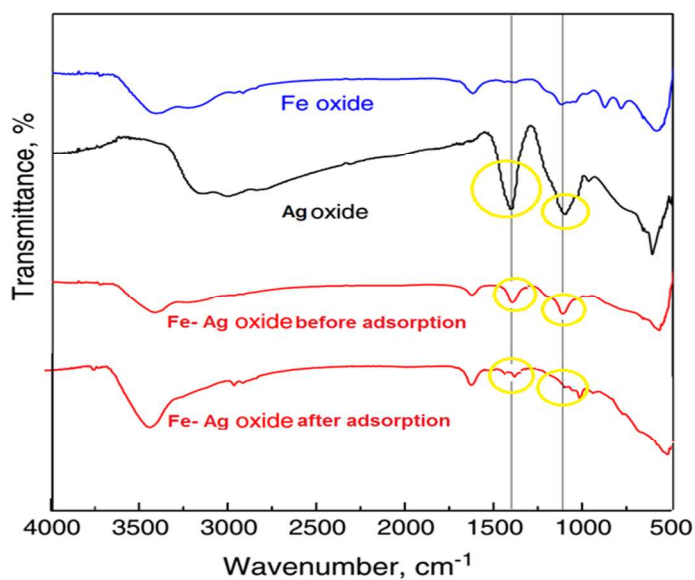


Fig.14. FT-IR spectra of Fe oxide, Ag oxide and Fe-Ag oxide before and after adsorption

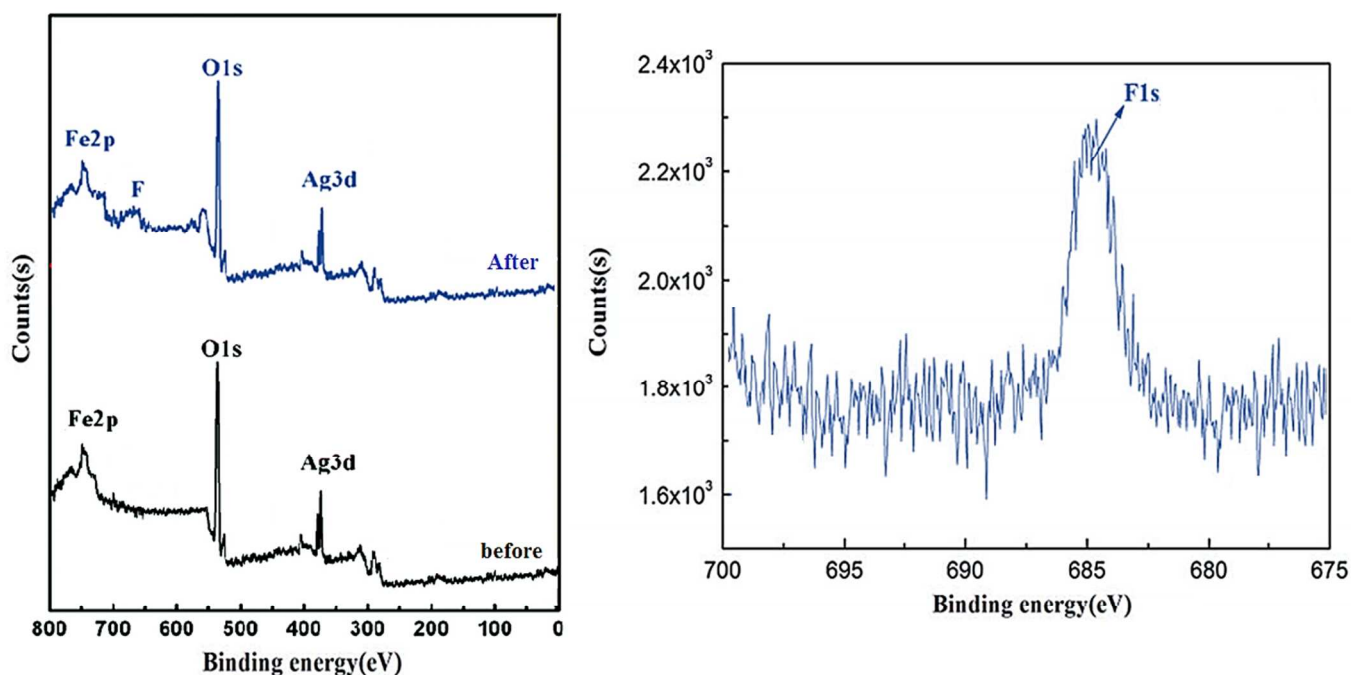


Fig.15. XPS spectra of Fe–Ag MBON (a) before and (b) after fluoride adsorption; XPS spectra of F 1s (c).

The mechanism of Fluoride adsorption on the surface of Fe-Ag as adsorbent before and after the sorption process were analyzed by XPS technique and the results are shown in Fig. 15. Comparing XPS analysis before and after the adsorption process shows that created a new peak with a binding energy ~ 685 eV which was assigned to F1s. Besides, the relative atomic ratios of XPS analysis (%) for Ag, O, Fe and F in adsorbents can confirm above context.

Table6. Atomic ratios of XPS analysis for the optimized synthesized sorbent before and after fluoride sorption.

Atomic ratios (%)	Ag	Fe	O	F
Fe—Ag oxide	14.28	7.56	81.21	0
Fe—Ag oxide- F	19.41	7.75	69.31	8.51

As seen in Table 6 amount of Fluoride on the surface of Fe—Ag MBON before sorption process equal to 0 while after adsorption increased to 8.51%, which confirmed that Fluoride had been uptake.

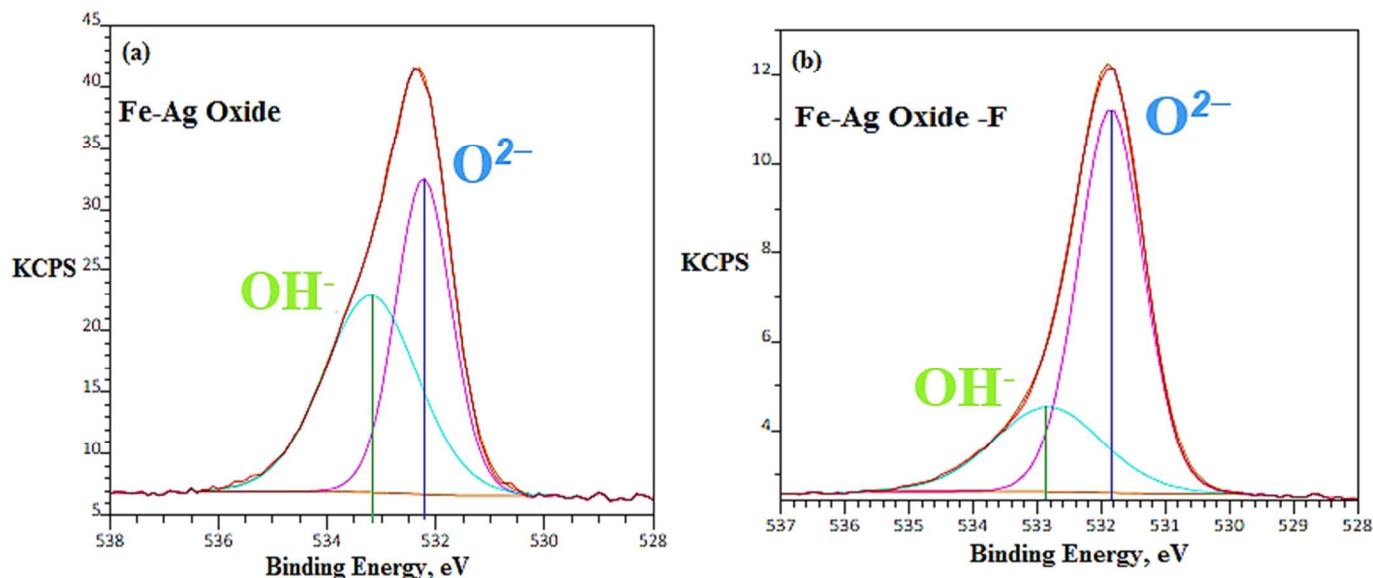


Fig 16. XPS (O₁S spectra) analyze of the optimized Fe- Ag and the fitted distribution of OH⁻ and O₂⁻ before (a) and after (b) fluoride adsorption

The O₁S spectra region of the optimized Fe—Ag MBON before and after the sorption process presented in Fig. 16 a and b. Two peaks in the O₁S spectra region are observed, one at ~532eV related to O₂⁻ that bonding with metal and other at ~533eV dedicated to OH⁻ groups on the surface of sorbent. As it can be seen the OH⁻ groups on the surface of Fe—Ag MBON decreased after Fluoride sorption. The summarized details of O₁S spectra region are given in Table 7.

Table7. Distribution of O²⁻ and OH⁻ in XPS (O₁S spectra) analyze for optimized Fe—Ag MBON as adsorbents before and after fluoride sorption.

Sample	Peak	B.E(eV)	FWHM(eV)	Percent (%)
Fe—Ag oxide	O ²⁻	532.2	1.72	41.65
	OH ⁻	533.21	1.65	57.61
Fe—Ag oxide- F	O ²⁻	531.80	2.38	97.87
	OH ⁻	532.82	1.83	1.53

Table 7 shows after defluorination the relative area of hydroxyl dropped sharply from 57.61 % to 1.53 % and the area ratio for the peak at ~532eV allocated to O₂⁻ increased from 41.65 % to 97.87 %. The decrease of OH⁻ group percentage attributed to the substitution of hydroxyl by Fluoride during the adsorption process. Thus, the XPS analysis also suggested OH⁻ groups onto the surface of Fe—Ag MBON played a significant role in Fluoride adsorption, which was in accommodation with the results of the FTIR studies.

4. Conclusions

In this work, we were carried out several experiments to investigate the performance of Fe–Ag MBON as an adsorbent for removal of Fluoride. The Fe–Ag MBON was synthesized in a molar ratio of 3:1 at ~10 nm diameter (micro porous) and a suitable magnetic properties. The optimum condition for defluoridation (removal efficiency =100%) obtained in pH= 3, 20 min contact time and 0.5 gr/L sorbent dosage at 293 °K. Therefore synthesized sorbent can be used in the water and wastewater advance treatment confidently with no need of further filtering and centrifugation. The adsorption equilibrium data followed well with Langmuir isotherm models. The kinetic study shows that system has better coordination with pseudo second-order models. Thermodynamic study illustrates that sorption of Fluoride is feasible, exothermic and spontaneous in nature. The presence co-existing anions except PO_4^{3-} and HCO_3^- have not a significant effect on F^- removal.

Acknowledgment

This study was done by financial support of Tehran University of Medical Sciences and Iranian Nano Technology Initiative Council.

5. References

- [1] H. Jin, Z. Ji, J. Yuan, J. Li, M. Liu, C. Xu, J. Dong, P. Hou, S. Hou, Research on removal of fluoride in aqueous solution by alumina-modified expanded graphite composite, *Journal of Alloys and Compounds* 620 (2015) 361-367.
- [2] A. Bhatnagar, E. Kumar, M. Sillanpää, Fluoride removal from water by adsorption—a review, *Chemical Engineering Journal* 171 (2011) 811-840.
- [3] M. Habuda-Stanić, M.E. Ravančić, A. Flanagan, A Review on Adsorption of Fluoride from Aqueous Solution, *Materials* 7 (2014) 6317-6366.
- [4] J. Wang, D. Kang, X. Yu, M. Ge, Y. Chen, Synthesis and characterization of Mg–Fe–La trimetal composite as an adsorbent for fluoride removal, *Chemical Engineering Journal* 264 (2015) 506-513.
- [5] T. Nur, P. Loganathan, T. Nguyen, S. Vigneswaran, G. Singh, J. Kandasamy, Batch and column adsorption and desorption of fluoride using hydrous ferric oxide: Solution chemistry and modeling, *Chemical Engineering Journal* 247 (2014) 93-102.
- [6] S. Jagtap, M.K. Yenkie, N. Labhsetwar, S. Rayalu, Fluoride in drinking water and defluoridation of water, *Chemical reviews* 112 (2012) 2454-2466.
- [7] J.-Q. Zhu, Y.-J. Si, L.-Y. Cheng, B.-Z. Xu, Q.-W. Wang, X. Zhang, H. Wang, Z.-P. Liu, Sodium fluoride disrupts DNA methylation of H19 and Peg3 imprinted genes during the early development of mouse embryo, *Archives of toxicology* 88 (2014) 241-248.
- [8] V. Hernandez-Montoya, L.A. Ramirez-Montoya, A. Bonilla-Petriciolet, M.A. Montes-Moran, Optimizing the removal of fluoride from water using new carbons obtained by modification of nut shell with a calcium solution from egg shell, *Biochemical Engineering Journal* 62 (2012) 1-7.
- [9] N.A. Ingle, H.V. Dubey, N. Kaur, I. Sharma, Defluoridation techniques: Which one to choose, *Journal of Health Research and Reviews* 1 (2014) 1.
- [10] N.K. Labhsetwar, S.J. Lunge, A.K. Bansiwala, P.K. Labhsetwar, S.S. Rayalu, S.R. Wate, Technological Developments in Water Defluoridation, *Aquananotechnology: Global Prospects* (2014) 317.
- [11] I. Saha, A. Ghosh, D. Nandi, K. Gupta, D. Chatterjee, U.C. Ghosh, β -Cyclodextrin modified hydrous zirconium oxide: Synthesis, characterization and defluoridation performance from aqueous solution, *Chemical Engineering Journal* 263 (2015) 220-230.
- [12] D. Dayananda, V.R. Sarva, S.V. Prasad, J. Arunachalam, P. Parameswaran, N.N. Ghosh, Synthesis of MgO nanoparticle loaded mesoporous Al₂O₃ and its defluoridation study, *Applied Surface Science* 329 (2015) 1-10.
- [13] S.-F. Chen, H.-Z. Zhang, Z.-L. Wang, X.-L. Tang, L.-N. Pan, Removal of Fluoride from Water by Activated Natural Zeolite Coated with Chitosan, *Environmental Science & Technology* 7 (2012) 018.
- [14] K. Pandi, N. Viswanathan, In situ precipitation of nano-hydroxyapatite in gelatin polymatrix towards specific fluoride sorption, *International journal of biological macromolecules* 74 (2015) 351-359.
- [15] A.D. Atasoy, M.O. Sahin, Adsorption of fluoride on the raw and modified cement clay, *CLEAN–Soil, Air, Water* 42 (2014) 415-420.
- [16] J. Zhang, N. Chen, Z. Tang, Y. Yu, Q. Hu, C. Feng, A study of the mechanism of fluoride adsorption from aqueous solutions onto Fe-impregnated chitosan, *Physical Chemistry Chemical Physics* (2015).
- [17] S.M. Prabhu, S. Meenakshi, Chemistry of defluoridation by one-pot synthesized dicarboxylic acids mediated polyacrylamide–zirconium complex, *Chemical Engineering Journal* 262 (2015) 224-234.
- [18] E. Kumar, A. Bhatnagar, W. Hogland, M. Marques, M. Sillanpää, Interaction of inorganic anions with iron-mineral adsorbents in aqueous media—A review, *Advances in colloid and interface science* 203 (2014) 11-21.
- [19] J. García-Sánchez, M. Solache-Ríos, M. Alarcón-Herrera, V. Martínez-Miranda, Removal of fluoride from well water by modified iron oxides in a column system, *Desalination and Water Treatment* (2014) 1-9.
- [20] X. Wu, Y. Zhang, X. Dou, B. Zhao, M. Yang, Fluoride adsorption on an Fe–Al–Ce trimetal hydrous oxide: characterization of adsorption sites and adsorbed fluorine complex species, *Chemical Engineering Journal* 223 (2013) 364-370.
- [21] G. Li, S. Gao, G. Zhang, X. Zhang, Enhanced adsorption of phosphate from aqueous solution by nanostructured iron (III)–copper (II) binary oxides, *Chemical Engineering Journal* 235 (2014) 124-131.
- [22] N. Chen, C. Feng, M. Li, Fluoride removal on Fe–Al-impregnated granular ceramic adsorbent from aqueous solution, *Clean Technologies and Environmental Policy* 16 (2014) 609-617.
- [23] S. Swain, T. Patnaik, P. Patnaik, U. Jha, R. Dey, Development of new alginate entrapped Fe (III)–Zr (IV) binary mixed oxide for removal of fluoride from water bodies, *Chemical Engineering Journal* 215 (2013) 763-771.
- [24] L. Chen, B.-Y. He, S. He, T.-J. Wang, C.-L. Su, Y. Jin, Fe–Ti oxide nano-adsorbent synthesized by co-precipitation for fluoride removal from drinking water and its adsorption mechanism, *Powder Technology* 227 (2012) 3-8.

- [25] W. Zhang, J. Fu, G. Zhang, X. Zhang, Enhanced arsenate removal by novel Fe–La composite (hydr) oxides synthesized via coprecipitation, *Chemical Engineering Journal* 251 (2014) 69-79.
- [26] Z. Marková, K.n.M. Šišková, J. Filip, J. Čuda, M. Kolář, K.r. Šafářová, I. Medřík, R. Zbořil, Air stable magnetic bimetallic Fe–Ag nanoparticles for advanced antimicrobial treatment and phosphorus removal, *Environmental science & technology* 47 (2013) 5285-5293.
- [27] W. Al-Saidi, H. Feng, K. Fichtorn, Adsorption of polyvinylpyrrolidone on Ag surfaces: Insight into the workings of a structure-directing agent, *APS March Meeting Abstracts*, 2012, pp. 6007.
- [28] M. Ghaedi, B. Sadeghian, A.A. Pebdani, R. Sahraei, A. Daneshfar, C. Duran, Kinetics, thermodynamics and equilibrium evaluation of direct yellow 12 removal by adsorption onto silver nanoparticles loaded activated carbon, *Chemical Engineering Journal* 187 (2012) 133-141.
- [29] W. Zhang, J. Fu, G. Zhang, X. Zhang, Enhanced arsenate removal by novel Fe–La composite (hydr)oxides synthesized via coprecipitation, *Chemical Engineering Journal* 251 (2014) 69-79.
- [30] S. Luo, S. Yang, C. Sun, J.-D. Gu, Improved debromination of polybrominated diphenyl ethers by bimetallic iron–silver nanoparticles coupled with microwave energy, *Science of the Total Environment* 429 (2012) 300-308.
- [31] Z. Zheng, S. Yuan, Y. Liu, X. Lu, J. Wan, X. Wu, J. Chen, Reductive dechlorination of hexachlorobenzene by Cu/Fe bimetal in the presence of nonionic surfactant, *Journal of hazardous materials* 170 (2009) 895-901.
- [32] Z. Markova, K. Siskova, J. Filip, J. Cuda, M. Kolar, K. Safarova, I. Medrik, R. Zboril, Air Stable Magnetic Bimetallic Fe-Ag Nanoparticles for Advanced Antimicrobial Treatment and Phosphorus Removal, *Environmental science & technology* (2013).
- [33] J.P.T. Baú, C.E. Carneiro, I.G. de Souza Junior, C.M. de Souza, A.C. da Costa, E. di Mauro, C.T. Zaia, J. Coronas, C. Casado, H. de Santana, Adsorption of adenine and thymine on zeolites: FT-IR and EPR spectroscopy and X-ray diffractometry and SEM studies, *Origins of Life and Evolution of Biospheres* 42 (2012) 19-29.
- [34] K.J. Carroll, D.M. Hudgins, S. Spurgeon, K.M. Kemner, B. Mishra, M.I. Boyanov, L.W. Brown III, M.L. Taheri, E.E. Carpenter, One-pot aqueous synthesis of Fe and Ag core/shell nanoparticles, *Chemistry of Materials* 22 (2010) 6291-6296.
- [35] B. Kakavandi, R.R. Kalantary, M. Farzadkia, A.H. Mahvi, A. Esrafil, A. Azari, A.R. Yari, A.B. Javid, Enhanced chromium (VI) removal using activated carbon modified by zero valent iron and silver bimetallic nanoparticles, *Journal of Environmental Health Science and Engineering* 12 (2014) 115.
- [36] J. Ma, Y. Shen, C. Shen, Y. Wen, W. Liu, Al-doping chitosan–Fe (III) hydrogel for the removal of fluoride from aqueous solutions, *Chemical Engineering Journal* 248 (2014) 98-106.
- [37] H.-m. Cai, G.-j. Chen, C.-y. Peng, Z.-z. Zhang, Y.-y. Dong, G.-z. Shang, X.-h. Zhu, H.-j. Gao, X.-c. Wan, Removal of fluoride from drinking water using tea waste loaded with Al/Fe oxides: A novel, safe and efficient biosorbent, *Applied Surface Science* 328 (2015) 34-44.
- [38] A.B. Albadarin, Z. Yang, C. Mangwandi, Y. Glocheux, G. Walker, M. Ahmad, Experimental design and batch experiments for optimization of Cr (VI) removal from aqueous solutions by hydrous cerium oxide nanoparticles, *Chemical Engineering Research and Design* 92 (2014) 1354-1362.
- [39] K. Chu, Removal of copper from aqueous solution by chitosan in prawn shell: adsorption equilibrium and kinetics, *Journal of Hazardous Materials* 90 (2002) 77-95.
- [40] W. Ma, N. Zhao, G. Yang, L. Tian, R. Wang, Removal of fluoride ions from aqueous solution by the calcination product of Mg–Al–Fe hydrotalcite-like compound, *Desalination* 268 (2011) 20-26.
- [41] S. Swain, T. Patnaik, V. Singh, U. Jha, R. Patel, R. Dey, Kinetics, equilibrium and thermodynamic aspects of removal of fluoride from drinking water using meso-structured zirconium phosphate, *Chemical engineering journal* 171 (2011) 1218-1226.
- [42] K.S. Prasad, Y. Amin, K. Selvaraj, Defluoridation using biomimetically synthesized nano zirconium chitosan composite: Kinetic and equilibrium studies, *Journal of hazardous materials* 276 (2014) 232-240.
- [43] S. Swain, T. Patnaik, R. Dey, Efficient removal of fluoride using new composite material of biopolymer alginate entrapped mixed metal oxide nanomaterials, *Desalination and Water Treatment* 51 (2013) 4368-4378.
- [44] S.K. Nath, K.G. Bhattacharyya, Adsorption of Arsenite and Fluoride on Untreated and Treated Bamboo Dust, *Management of Natural Resources in a Changing Environment*, Springer2015, pp. 167-180.
- [45] D. Wan, Y. Liu, S. Xiao, J. Chen, J. Zhang, Uptake fluoride from water by caclined Mg–Al–CO₃ hydrotalcite: Mg/Al ratio effect on its structure, electrical affinity and adsorptive property, *Colloids and Surfaces A: Physicochemical and Engineering Aspects* 469 (2015) 307-314.
- [46] S. Deng, H. Liu, W. Zhou, J. Huang, G. Yu, Mn–Ce oxide as a high-capacity adsorbent for fluoride removal from water, *Journal of hazardous materials* 186 (2011) 1360-1366.

- [47] M. Barathi, A.S.K. Kumar, N. Rajesh, Efficacy of novel Al–Zr impregnated cellulose adsorbent prepared using microwave irradiation for the facile defluoridation of water, *Journal of Environmental Chemical Engineering* 1 (2013) 1325-1335.
- [48] D. Thakre, S. Jagtap, N. Sakhare, N. Labhsetwar, S. Meshram, S. Rayalu, Chitosan based mesoporous Ti–Al binary metal oxide supported beads for defluoridation of water, *Chemical Engineering Journal* 158 (2010) 315-324.
- [49] A. Ghosh, S. Chakrabarti, K. Biswas, U.C. Ghosh, Agglomerated nanoparticles of hydrous Ce (IV)+ Zr (IV) mixed oxide: Preparation, characterization and physicochemical aspects on fluoride adsorption, *Applied Surface Science* 307 (2014) 665-676.
- [50] L. Calvo, M.A. Gilarranz, J.A. Casas, A.F. Mohedano, J.J. Rodriguez, Denitrification of water with activated carbon-supported metallic catalysts, *Industrial & Engineering Chemistry Research* 49 (2010) 5603-5609.
- [51] O.S.G. Soares, J.J. Órfão, M.F.R. Pereira, Nitrate reduction in water catalysed by Pd–Cu on different supports, *Desalination* 279 (2011) 367-374.
- [52] Y. Yoshinaga, T. Akita, I. Mikami, T. Okuhara, Hydrogenation of nitrate in water to nitrogen over Pd–Cu supported on active carbon, *Journal of catalysis* 207 (2002) 37-45.
- [53] J. Jung, S. Bae, W. Lee, Nitrate reduction by maghemite supported Cu-Pd bimetallic catalyst, *Applied Catalysis B: Environmental* 127 (2012) 148-158.